The Astrophysical Journal, 803:94 (11pp), 2015 April 20 doi:10.1088/0004-637X/803/2/94

AUTOMATIC DETECTION ALGORITHM OF DYNAMIC PRESSURE PULSES IN THE SOLAR WIND

Pingbing Zuo[1], Xueshang Feng[1], Yanqiong Xie[2], Yi Wang[1], Huijun Li[2], and Xiaojun Xu[3]
[1] SIGMA Weather Group, State Key Laboratory of Space Weather, Center for Space Science and Applied Research, Chinese Academy of Sciences, Beijing, China; pbzuo@spaceweather.ac.cn, fengx@spaceweather.ac.cn
[2] College of Meteorology and Oceanography, PLA University of Science and Technology, Nanjing, China
[3] Institute of Space Science and Technology, Nanchang University, Nanchang, China
Received 2014 October 13; accepted 2015 February 15; published 2015 April 22

ABSTRACT

Dynamic pressure pulses (DPPs) in the solar wind are a significant phenomenon closely related to the solar-terrestrial connection and physical processes of solar wind dynamics. In order to automatically identify DPPs from solar wind measurements, we develop a procedure with a three-step detection algorithm that is able to rapidly select DPPs from the plasma data stream and simultaneously define the transition region where large dynamic pressure variations occur and demarcate the upstream and downstream region by selecting the relatively quiet status before and after the abrupt change in dynamic pressure. To demonstrate the usefulness, efficiency, and accuracy of this procedure, we have applied it to the *Wind* observations from 1996 to 2008 by successfully obtaining the DPPs. The procedure can also be applied to other solar wind spacecraft observation data sets with different time resolutions.

Key words: methods: data analysis – solar wind – solar–terrestrial relations

1. INTRODUCTION

In interplanetary (IP) space, some small-scale plasma structures with abrupt increase or decrease in plasma dynamic pressure are frequently observed. Found from the high resolution data, they usually have a very sharp front with dynamic pressure changing abruptly in a pulse form on timescales of seconds to a few minutes (Dalin et al. 2002). They are usually called solar wind dynamic pressure pulses (DPPs) or dynamic pressure fronts when they could be isolated in the sense that there are only small variations in the preceding and succeeding regions.

The abrupt changes in solar wind dynamic pressure affect the energy and momentum transported from the solar wind to the magnetosphere–ionosphere coupling system, and as a result, cause various types of disturbances particularly under the condition of southward interplanetary magnetic fields (Lyon 2000). Many papers were devoted to studying the responses of the main plasma regions in the magnetosphere and ionosphere to large positive DPPs usually associated with strong IP shocks or other discontinuities. The magnetospheric compression resulting from a large pressure front may involve sudden changes of not only the magnetopause current system but also the tail current and reconnection-related field-aligned currents (Zesta et al. 2000, p. 127), which in sequence cause a sudden increase in the ground geomagnetic field (Russell et al. 1994; Liou et al. 2004), disturbances in the magnetic field at the geosynchronous orbit (Sanny et al. 2002; Wing et al. 2002; Lee & Lyons 2004; Wang et al. 2007), and disturbances in the magnetic field at the tail lobe (Fairfield & Jones 1996; Ostapenko & Maltsev 1998; Collier et al. 1998; Kim et al. 2004). It can trigger the sudden enhancement of the flux of the energetic particles nearly simultaneously in both the dayside and nightside at the geosynchronous orbit (Lee et al. 2004, 2005). The flux enhancements of relativistic electrons and energetic ions in the magnetosphere as effects of the increase in dynamic pressure were also observed (Li et al. 2003; Zong et al. 2009). The reported ionosphere responses to the DPPs are global including auroral zone expansion (Lyons et al. 2000, 2005; Boudouridis et al. 2003; Zhou et al. 2013), enhancements in polar cap convection, ionospheric currents, and auroral precipitation (Chua et al. 2001). In conclusion, the DPPs are very geoeffective, which makes DPPs draw considerable attention in the field of solar-terrestrial connection during the last decade.

DPPs may be created under specific solar wind conditions (Dalin et al. 2002) or may be caused by plasma instabilities, magnetic reconnection, or plasma turbulence (Zuo et al. 2006; Riazantseva et al. 2007). They are also likely born in the solar atmosphere and may be modified by turbulent processes in the flow during transport in IP space. The investigation of the origin of the observed DPPs and their evolution in IP space is also important since it contributes to understanding the solar wind features and the rich physical processes in IP space.

To detect DPPs rapidly from the solar wind plasma data to benefit the research on the DPP-related scientific problems, an automated DPP-hunting computer procedure has been developed. To this end, the code will not only identify and isolate the special structure but also automatically determine the DPP transition region and select appropriate preceding and succeeding reference data points as well for which there are very small variations in solar wind dynamic pressure to represent the quiet plasma status before and after the pressure change.

High-resolution measurements indicate that the pressure changes can occur on timescales from a few seconds to many minutes. The code can be used to hunt for DPPs of arbitrary ramp length and arbitrary pressure variation amplitude by adjusting its criteria. Strong DPPs with very large pressure change are most geoeffective and are able to affect the near-Earth environment intensely. Thus the code also benefits large-DPP-related space weather warnings or forecasting. In this paper, we present the procedure for identifying and defining the upstream, downstream, and the transition region. The effectiveness of this code is validated by *Wind* high-resolution measurements covering the 23rd solar cycle.

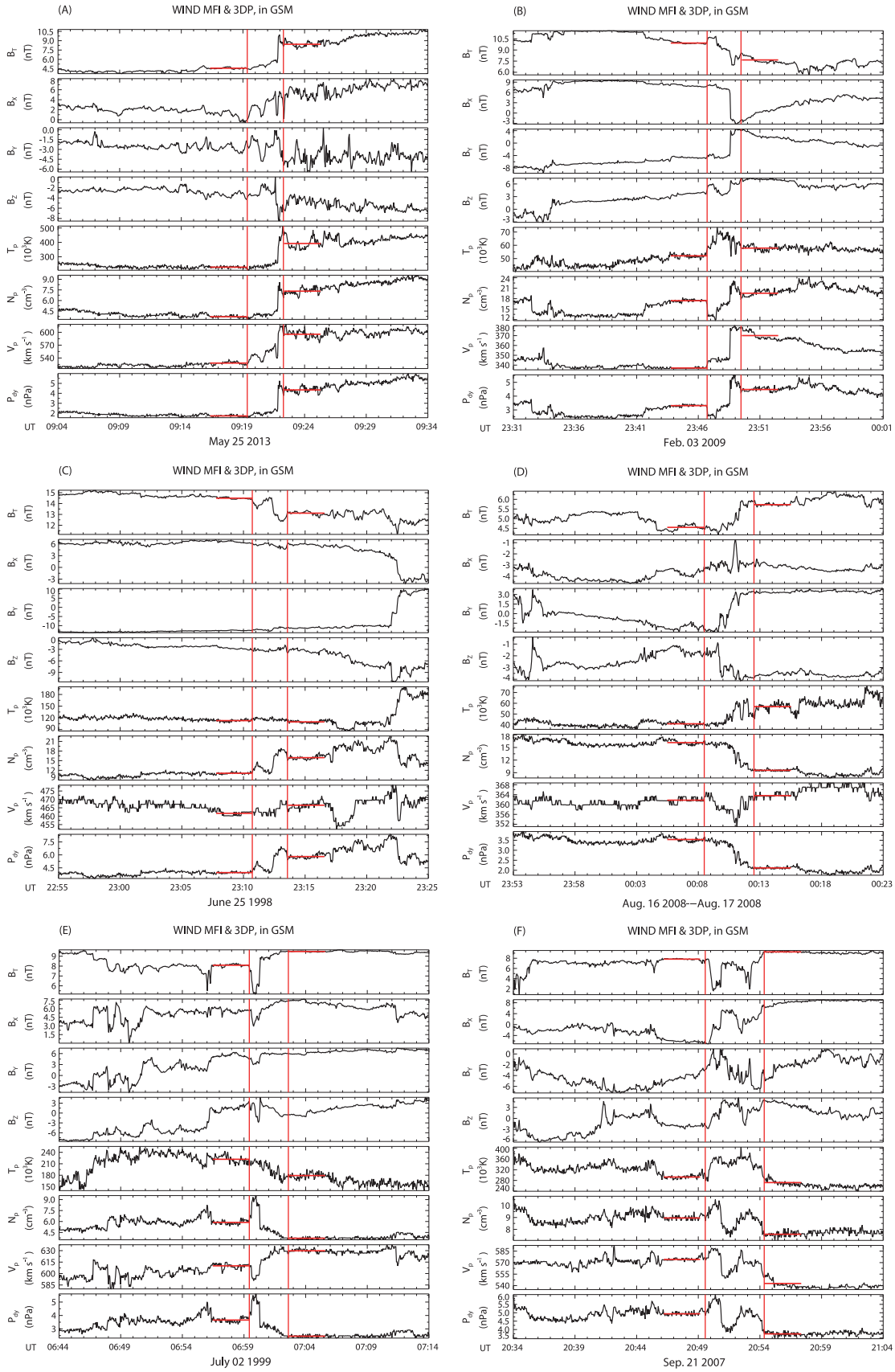

Figure 1. Examples of dynamic pressure pulses (DPPs) in the solar wind detected by *Wind*.

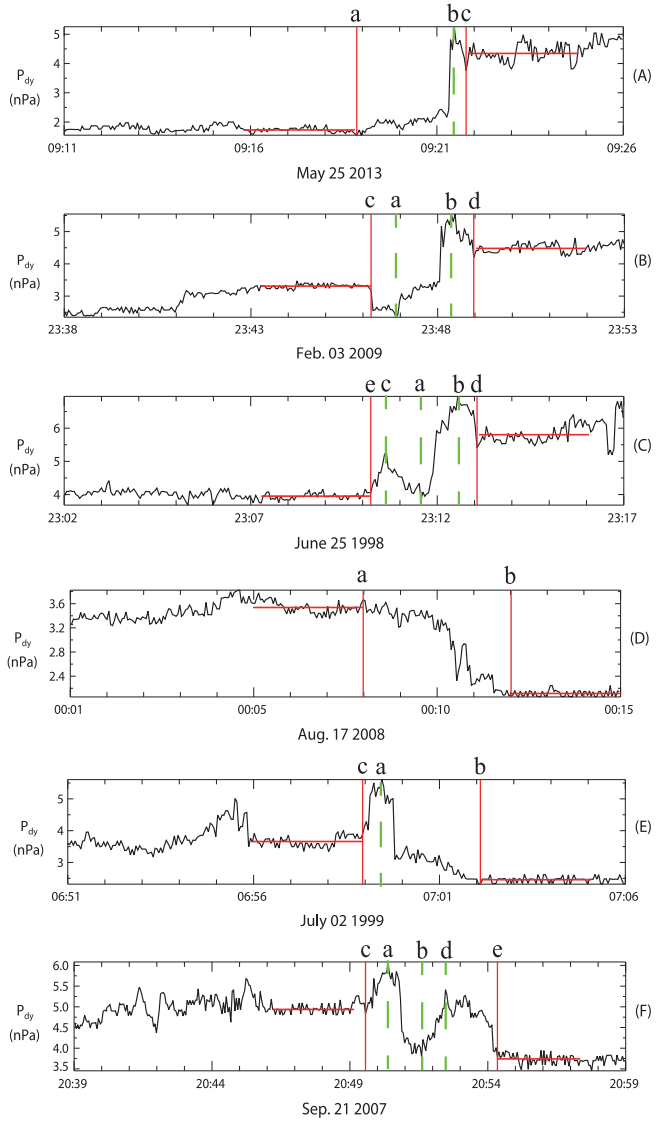

Figure 2. Fine dynamic pressure variations in the vicinity of each typical DPP presented in Figure 1. The red lines denoted the final results of defining the upstream, the transition region, and the downstream using the code.

2. THREE-STEP DETECTION ALGORITHM

The code is designed to hunt for sudden changes in the solar wind dynamic pressure $P_{\rm dy}$ from the in situ spacecraft plasma data. Although the solar wind dynamic pressure is contributed by all the species including protons, alpha ions, electrons, and other minor ions, the proton dynamic pressure $m_p\, n_p\, V_p^2$ is dominant in the IP medium, where m_p, n_p, and V_p are the proton mass, number density, and bulk speed, respectively. Thus we only survey the change in proton dynamic pressure to identify DPPs in this code. Here we take the high-resolution plasma data from the 3DP instrument on board the *Wind* spacecraft (Lin et al. 1995) as code tests. The data used are nominally 3 s resolution and are available unintermittently through solar cycle 23.

By definition, it requires that the solar wind dynamic pressure increase or decrease abruptly within a very short interval across the DPPs and stay relatively stable on both sides. Accordingly, the selection of the DPP events is guided by the following criteria. (1) The dynamic pressure difference

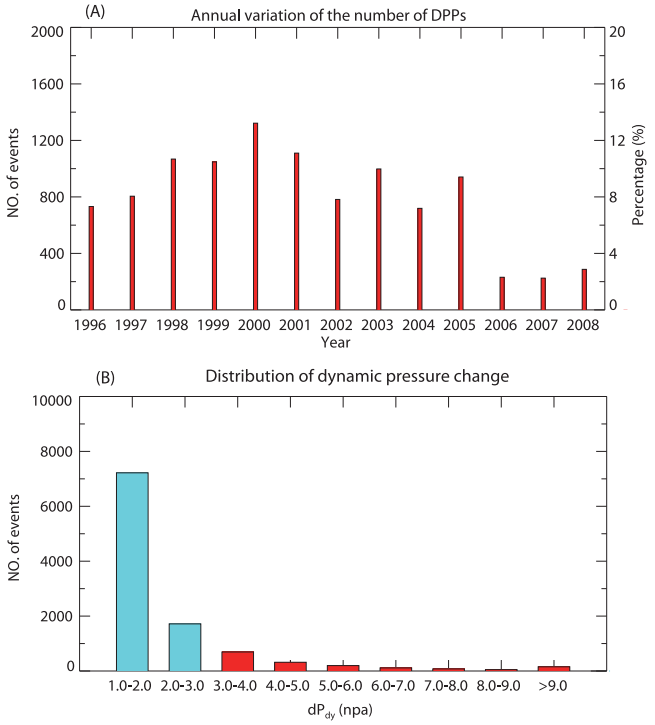

Figure 3. Annual variation of the number of dynamic pressure pulses (DPPs) in the solar wind detected by *Wind* in 1996–2008 (A), and the distribution of dynamic pressure change from upstream to downstream (B).

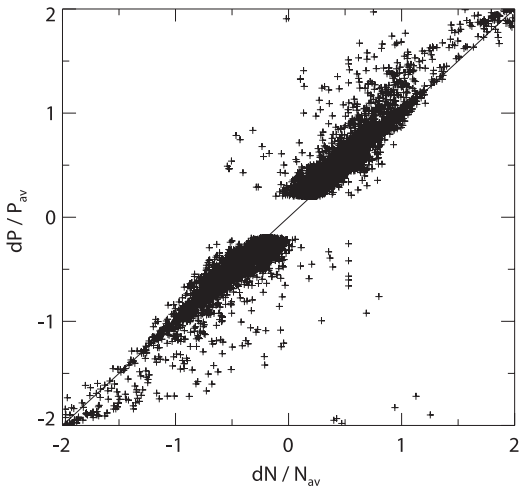

Figure 4. Scatter plot on the magnitude of the relative dynamic pressure changes and the magnitude of the relative density changes to show their dependence.

on both sides exceeds a given threshold value dp_0. (2) The thickness of the pressure front is required to be small according to the definition of rapid pressure change. The crossing time of the DPP transition region should be less than a given time dt_0. (3) It should be isolated in the sense that only small variations in plasma parameters occur in the preceding and succeeding 3 minutes. Since the data resolution is very high, the 3 minute region can be representative for the status before and after the pressure front. The relatively quiet regions are called the upstream and the downstream below. The code demands that the variation amplitude of the dynamic pressure in the upstream region and in the downstream region is less than 0.6 times the

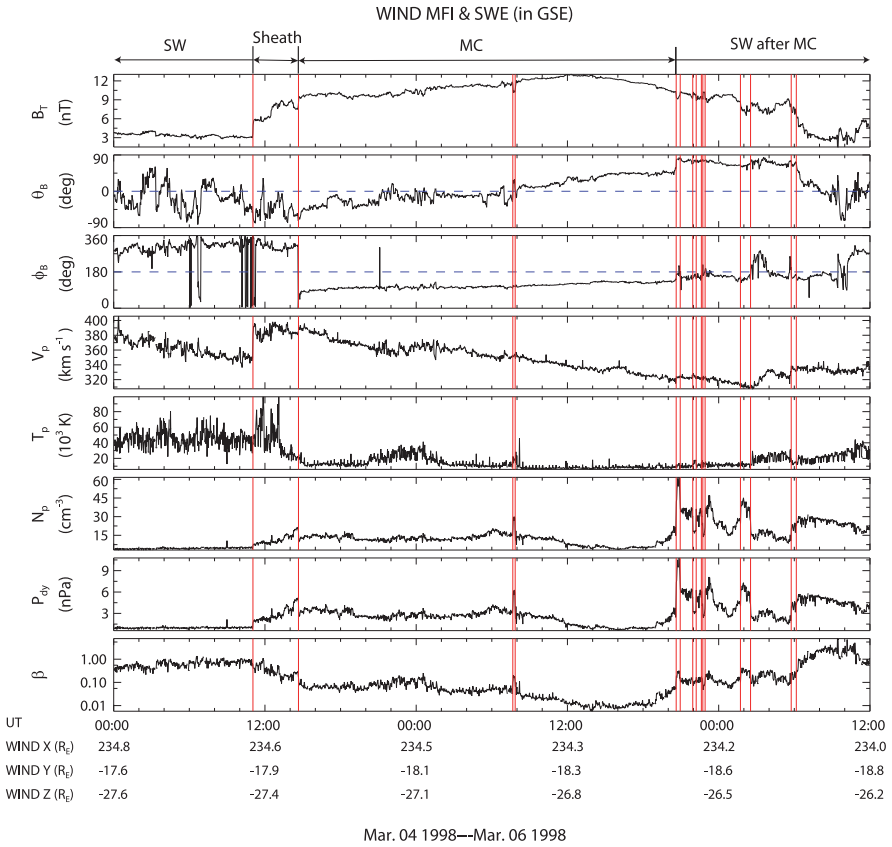

Figure 5. Magnetic field and plasma parameters from *Wind* observations in the interval between 00 UT on 1998 March 4 and 12 UT on 1998 March 6 with the passage of a typical magnetic cloud (MC). The code-detected DPPs are labeled with red vertical lines.

change amplitude in the transition region. Moreover, the square deviation of $P_{\rm dy}$ in the upstream and in the downstream is less than 0.6 times the corresponding average value. The threshold value dp_0 and dt_0 can be selected according to the research issues under investigation.

Figure 1 gives six typical examples of DPPs obtained by the automatic searching procedure. The panels from top to bottom show the magnetic field magnitude and the three magnetic components in GSM coordinates, the proton temperature, the proton number density, the solar wind bulk speed, and the proton dynamic pressure, respectively. The code-identified transition region is bounded by two vertical red solid lines. The upstream and downstream regions are marked by the red transverse lines that are situated at the locations of the average of each plasma and magnetic field parameter. Sudden pressure changes are usually accomplished by abrupt changes in magnetic field magnitude and direction. The code only captures the change in the dynamic pressure. If the dynamic pressure increases from upstream to downstream, we call it positive DPP (see Figures 1(a)–(c)); otherwise we call it negative DPP (see Figures 1(d)–(f)). It can be seen that the change of the dynamic pressure within the transition region may be very complicated, and the dynamic pressures are relatively quiet in the adjacent upstream and downstream regions. Sudden changes in magnetic field together with jumps in plasma parameters such as the ion flux or the dynamic pressure are often associated with MHD discontinuities including tangential discontinuities, rotational discontinuities with anisotropic thermal pressure, and shocks (e.g., Saka & Kitamura 1976; Wu et al. 1993; Dalin et al. 2002; Riazantseva et al. 2005, 2007; Neugebauer 2006). Some identified DPPs can be classified into these types of discontinuities. Figure 1(a) shows a typical IP shock that includes the foot, ramp, and the overshoot structure in the transition region. Figure 1(f) displays a magnetic hole structure for which the magnetic field decreases to a minimum then is recovered and transitioned to another state. The magnetic field change is accompanied by a reverse change in the dynamic pressure. Across the magnetic hole, the dynamic pressure decreases from 5.0 to 3.5 nPa. In addition, there are very small dynamic pressure variations in the adjacent regions of the magnetic hole. Here, this type of structure is also regarded as the DPP by definition. In the following, we will present how the code works in these cases in Figures 1(a)–(f).

The automatic detection of DPPs is designed below in a three-step manner.

(1) Step 1: search the structures with sudden change in dynamic pressure for DPP candidates. Although the dynamic pressure change may be very complicated in the transition region of a DPP, we can always find the locations of the maximum and minimum dynamic pressure in this region. In other words, we can easily verify the existence of one DPP by capturing the corresponding quick change region bounded by these two pressure peaks. The data of proton dynamic pressure $p_{dy} = m_p n_p V_p^2$ are scanned by using a sliding window with a size equal to dt_0, and the minimum $p_{\rm min}$ and maximum $p_{\rm max}$ are calculated. If the variation amplitude, i.e., $dp_{\rm ramp} = p_{\rm max} - p_{\rm min}$, is larger than $\frac{2}{3}dp_0$, it is recorded as a potential DPP. The front and rear boundaries of the DPP transition region are temporarily recorded as the location of two pressure peaks in the window. The window is shifted point by

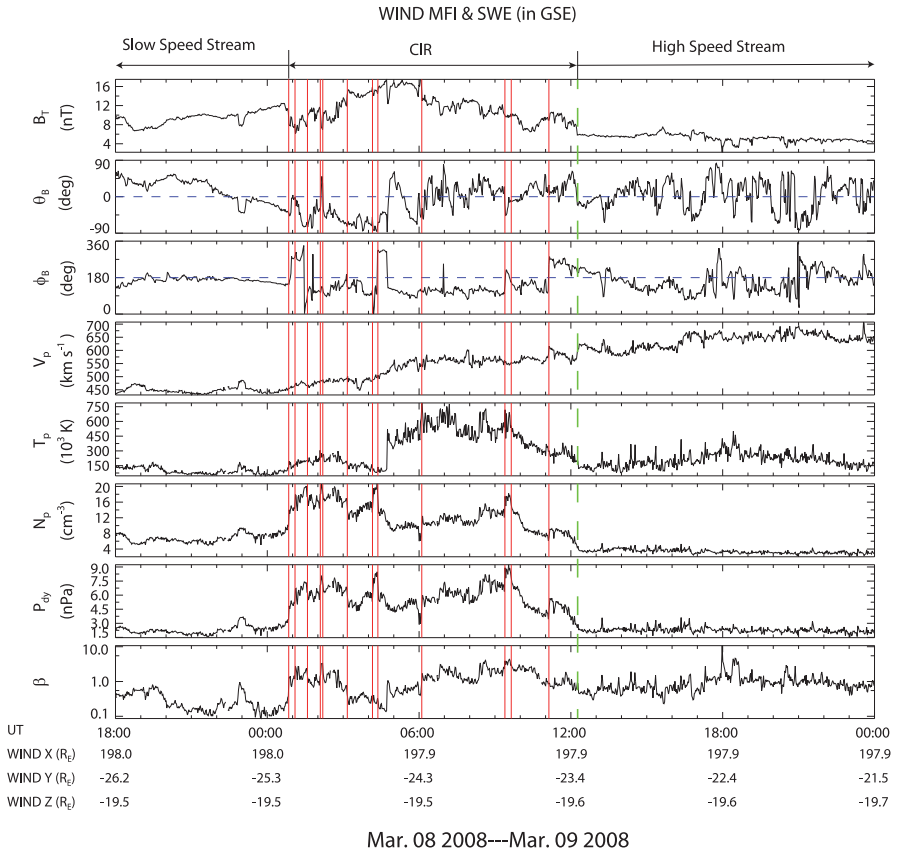

Figure 6. Magnetic field and plasma parameters of *Wind* observations in the interval between 00 UT on 2008 March 8 and 24 UT on 2008 March 9 with the passage of a corotating interaction region (CIR). The code-detected DPPs are labeled with red vertical lines. The green line is labeled as the rear boundary of the CIR which is not detected as a DPP by the code.

point and then the process is repeated for the entire data set. After the data are processed in this manner, we may get some overall same records by different window placements. In this case, we only keep one record.

(2) Step 2: select the qualified candidates and define their upstream and downstream regions. For each candidate obtained from Step 1, we inspect 120 data points before the front boundary of the transition region (corresponding to 6 minutes' time) to find a region with 60 consecutive data points (corresponding to 3 minutes' time) where the variation amplitude of dynamic pressure is lowest. This region is defined as the upstream region. Likewise, we inspect 120 data points after the rear boundary of the ramp and define the downstream by selecting a region with 60 consecutive data points where the variation amplitude of dynamic pressure is the lowest. Then the average, the variation amplitude, and the variance of the dynamic pressure in the upstream and downstream are calculated, denoted by p_1, δp_1, σ_1 (upstream) and p_2, δp_2, σ_2 (downstream), respectively. From criteria (1) and (3), we know that $|p_1 - p_2| > 1.0$ npa, $\sigma_1 < 0.6p_1$, $\sigma_2 < 0.6p_2$, $\delta p_1 < 0.6(|p_1 - p_2|)$, and $\delta p_2 < 0.6(|p_1 - p_2|)$. If the considered candidate does not meet these criteria, it is eliminated.

(3) Step 3: determine the transition region. After Step 2, the 3 minute relatively quiet regions before and after the dynamic pressure abruptly changes are selected as the upstream and downstream. Between the upstream and downstream, there may exist not only high-level pressure variations with large variation amplitude, but weak fluctuation of dynamic pressure before or after the high-level pressure variations. In addition, the high-level pressure variations sometimes are not monotonous. In this step, our purpose is to select the region merely containing the high-level dynamic pressure variations and define it as the transition region. First, we look for the locations corresponding to the maximum and minimum $p_{\rm dy}$ from the data between the upstream and downstream, and initially regard them as two boundaries of the transition region. Then if there are large pressure variations in the subregion between the transition region and the upstream or the subregion between this region and the downstream, the boundaries will be adjusted. Here, the criterion for so-called large pressure variations is that the variation amplitude δp is larger than 0.15 $p_{\rm max}$ in the subregion. We record the location of the peaks ($p_{\rm max}$ or $p_{\rm min}$) in the considered subregion. One of the peaks should be the boundary of the initially defined transition region. If the criterion is satisfied, the boundary is adjusted to the location of another peak recorded. In this way, we get the updated transition region. Then, the same process will be repeated for several times to get the final-determined transition region. Figure 2 shows the fine structure of the dynamic pressure for each case in Figure 1. The upstream and downstream determined after Step 2 are shown in the red horizontal lines. In Step 3, we first select the vertical lines a and b as the boundaries of the transition region and then they are updated step by step to the location denoted by the red vertical lines, i.e., the real boundaries of the transition region. For the case in Figure 1(a), the initial rear boundary line b is adjusted to line c, and the initial front boundary is kept unchanged since

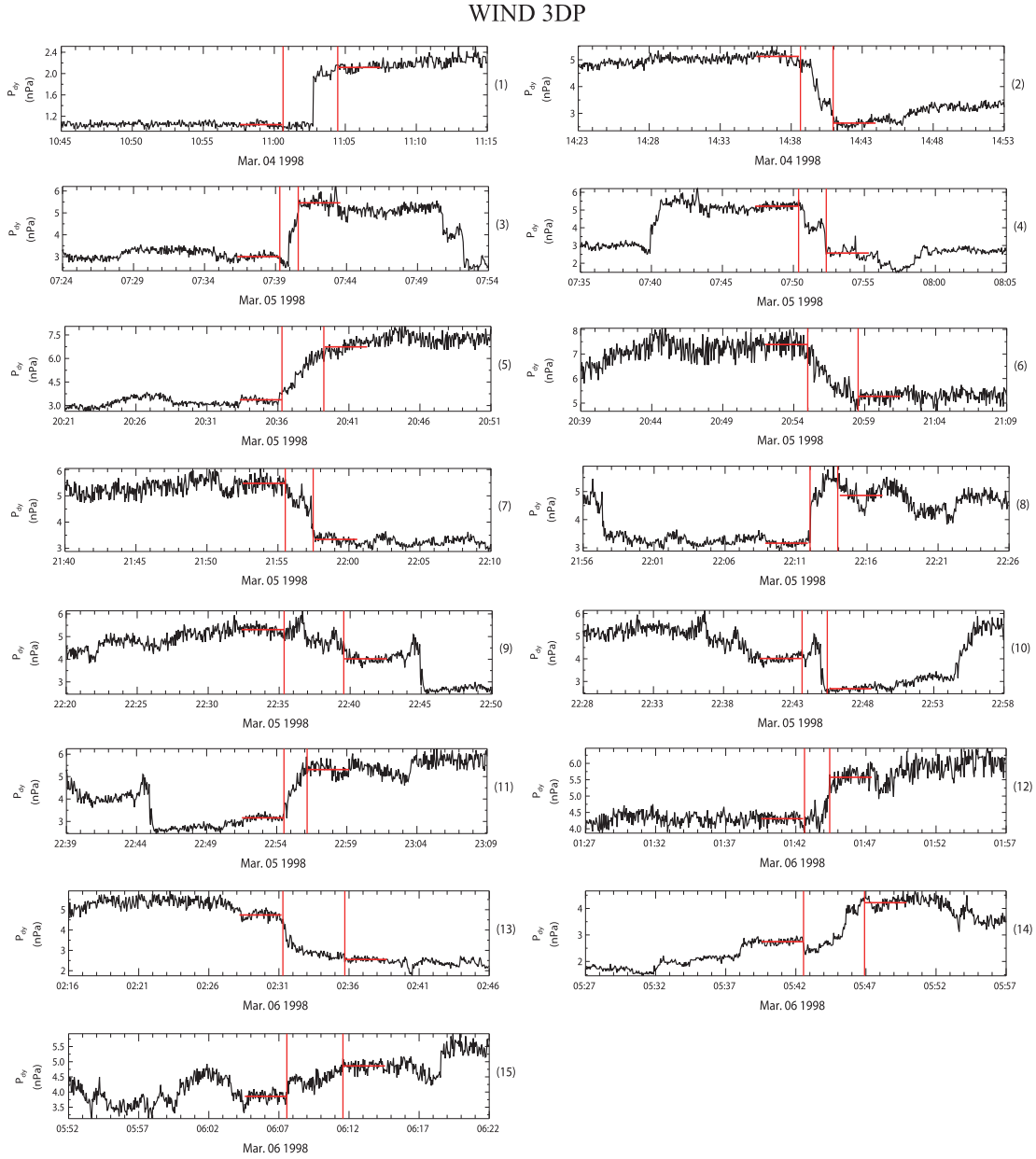

Figure 7. Fine dynamic pressure variation in a 30 minute window including each DPP detected in the interval between 00 UT on 1998 March 4 and 12 UT on 1998 March 6. The upstream and downstream defined by the code are labeled by the horizonal red lines, and the transition region is bounded by the vertical red lines.

there are no high-level pressure variations between line a and the rear boundary of the upstream; for the case in Figure 1(b), line a is adjusted to line c, and line b is adjusted to line d; for the case in Figure 1(c), line a is adjusted to line c, and then adjusted to line e by twice the adjustment, and line b is adjusted to line d; for the case in Figure 1(d), the boundaries line a and line b are not adjusted; for the case in Figure 1e, line a is adjusted to line c, while line b remains unchanged; for the case in Figure 1(f), line a is adjusted to line c, line b is adjusted to line d and then is adjusted to line e. It should be noted that sometimes there are gaps among the upstream, transition region, and downstream (see the example in Figure 2(f) and some cases in the following figures) especially in the wave-like plasma region or when some turbulences occur in the interval. Therefore it is not proper to simply regard the region between the upstream and downstream as the transition region. It can be seen from Figure 2, the transition region as well as the upstream and downstream region for each case can be reasonably determined by the three-step procedure.

3. CODE TEST

In order to test the feasibility of this DPP detection algorithm, we have applied it on the continuous measurements of *Wind* from 1996 to 2008, which cover the entire solar cycle 23. The program is repeatedly run on the *Wind* daily high-resolution 3DP data to automatically search the qualifying DPPs for which the dynamic pressure changes suddenly by at least 1 nPa in less than 5 minutes, that is, in the code, the threshold value of criteria dp_0 is given as 1 nPa, and dt_0 is set to be equal to 5 minutes. As a result, in total, we get more than 10,000 events with an average occurrence frequency of 2.2 events per day. It took less than 4 days to run the code on the 13 yr level-2 *Wind* data on a common PC with a CPU

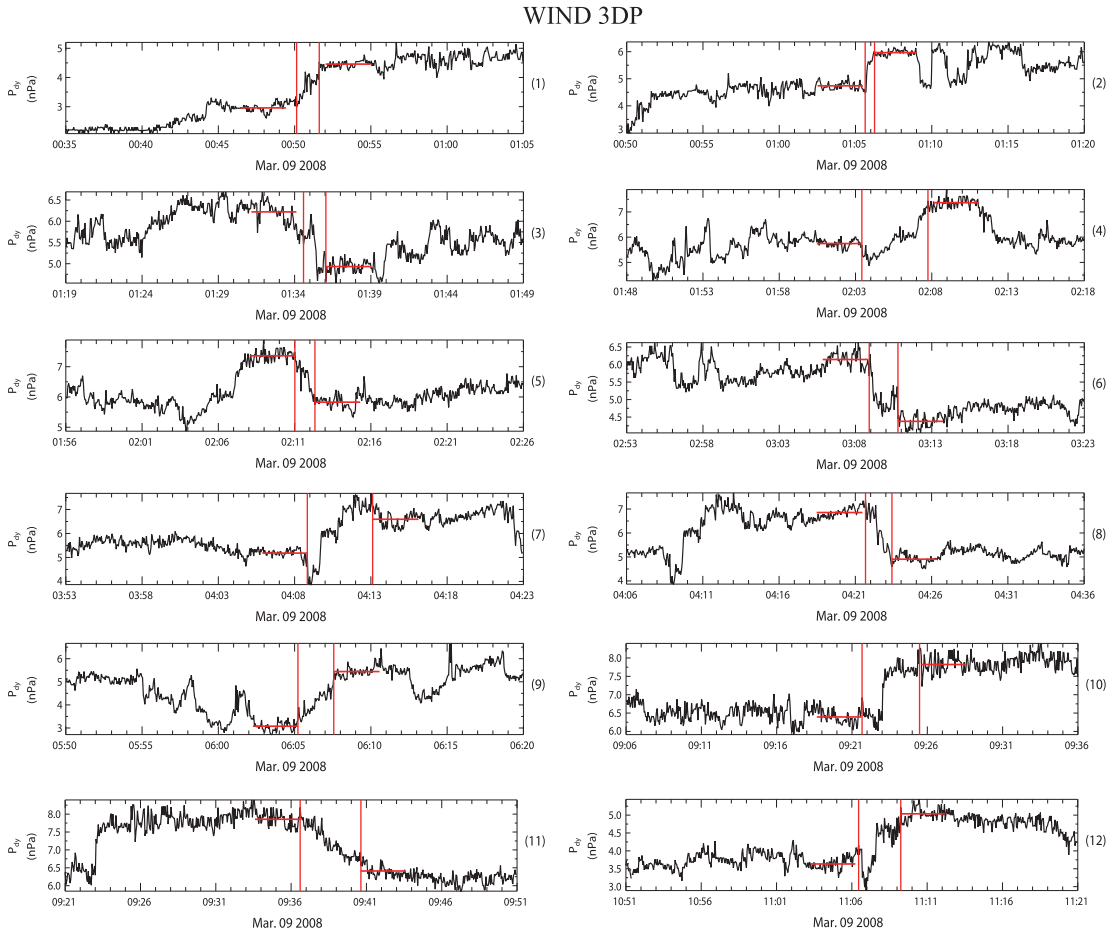

Figure 8. Fine dynamic pressure variation in a 30 minute window including each DPP detected in the interval between 00 UT on 2008 March 8 and 24 UT on 2008 March 9. The upstream and downstream defined by the code are labeled by the horizonal red lines, and the transition region is bounded by the vertical red lines.

frequency of 2.40 GHz and a memory of 4.0 GB, which demonstrates its efficiency. Figure 3(A) presents the number of all the detected DPP events in each year. The occurrence frequency in solar maximum during 2000–2001 (3.4 events per day) is obviously larger than that in solar minimum during 1996–1997 (2.2 events per day) and during 2007–2008 (0.7 event per day). It seems that the annual distribution of DPPs depends on the phase of the solar cycle. The distributions of the amplitudes of the dynamic pressure changes from upstream to downstream are presented in Figure 3(B). The most probable dynamic pressure changes are 1.0–2.0 nPa. The majority of dynamic pressure changes (about 70% of the events) are in the range of 1.0–3.0 nPa. There is a long tail beyond 3.0 nPa where the largest DPP is distributed. For a tiny minority of events, the pressure change is even greater than 30 nPa (not shown here). Although the largest DPPs account for a relatively small proportion of the total, they are the most geoeffective. Moreover, they usually are associated with large solar wind disturbances which makes them the potential indicators of a corresponding space weather event (Zastenker & Borodkova 1991).

Dalin et al. (2002) surveyed the DPPs based on nearly 3 yr of high time-resolution solar wind data from Interball-1 (in 1996 and 1998) and IMP 8 (in 1979). It is indicated that the dynamic pressure change for DPPs results mainly from the density change. Here we try to re-investigate this issue based on huge samples identified from *Wind* in the 23rd solar cycle. The magnitude of relative pressure changes ($dP_{\rm dy}/P_{\rm av}$, where $dp_{\rm dy}$ is the pressure change from upstream to downstream and $P_{\rm av}$ is the average of the upstream and downstream dynamic pressure) and the magnitude of the relative density changes ($dn/n_{\rm av}$, where dn is the number density change and $n_{\rm av}$ is the average of the density) are compared. Figure 4 shows the scatter plot of all the events. It can be seen that the majority of points (over 90%) lie close to the line of equality. The correlation coefficient between $dP_{\rm dy}/P_{\rm av}$ and $dn/n_{\rm av}$ is 0.98. Thus it confirms that the abrupt dynamic pressure changes are mainly dominated by the density changes.

Previous studies have indicated that DPPs are not distributed homogeneously but occur in groups in the solar wind (Dalin et al. 2002). The near-Earth solar wind can be divided into three types according to its origins and characteristics: (1) high speed streams associated with coronal holes at the Sun and the resulting corotating interaction region, (2) slow speed solar wind, and (3) transient flows including interplanetary coronal mass ejections, associated driven shocks, and the sheath regions (Richardson & Cane 2012). Analysis of the samples we searched indicates that the DPPs can be found in all three types of solar wind. Now we utilize the code to analyze the DPPs during two time intervals including all three types of solar wind when the DPPs occur in groups. To demonstrate the code accuracy, two questions need to be answered: (1) whether the code can reasonably give the transition region as well as the

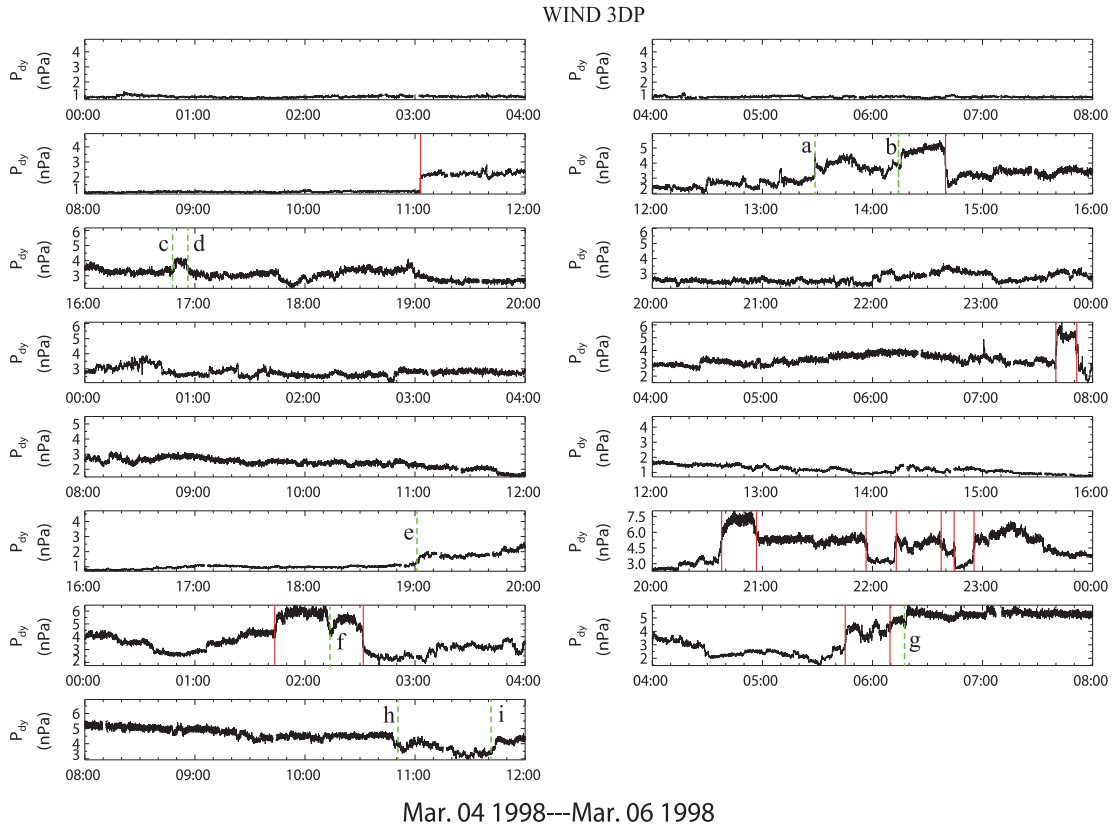

Figure 9. Dynamic pressure data from the *Wind* 3DP in the interval between 00 UT on 1998 March 4 and 12 UT on 1998 March 6 shown in 15 subfigures. The code-detected DPPs are denoted with red lines. The candidate DPPs from visual inspection are denoted with green lines.

corresponding upstream and downstream for each identified event and (2) whether the code misses any qualifying event. Figure 5 shows the *Wind* observations during the passage of a typical magnetic cloud (MC) and the disturbed preceding and succeeding solar wind from 00 UT on 1998 March 4 to 12 UT on 1998 March 6 (interval A). From top to bottom are shown the magnitude field and the magnetic directional angle, solar wind speed, the proton temperature, number density and the proton dynamic pressure, and the plasma β parameter, respectively. During the two and a half days, 15 DPPs were detected by our code. The position of each DPP is marked in the figure using red vertical lines. The MC can be identified from the strong and rotation magnetic field and the lower proton temperature. A fast forward shock is driven by the MC, which is also identified as a positive DPP. Between the shock and the MC is the turbulent sheath region. It can be seen that most DPPs are detected in the post MC region. The dynamic pressure is relatively stable within the MC so that only two DPPs exist within the smooth structure. Figure 6 presents the data during the interval from 18:00 UT on 2008 March 8 to 24:00 UT on 2008 March 9 (interval B) when a CIR was detected by *Wind*. The CIR is the region of interaction between the high-speed solar wind stream and the front low-speed stream. At the top of the figure, the slow speed stream, the high speed stream, and the CIR intervals are indicated by horizontal arrows. Near 1 AU, a forward–reverse shock pair has not yet formed, but it usually can be found in the edges of the CIR at further distance from the solar center beyond 2 AU. Here, the CIR boundaries are two pressure pulse structures, one of which is identified as a DPP at around 00:50 UT on 2008 March 9, but for another one, the transition region is too long (more than 8 minutes crossing) so that it does not meet our selection criteria for DPPs (see the green dashed line). In total, we get 12 DPPs in this interval, all of which are distributed within the CIR region.

Figures 7 and 8 present the fine dynamic pressure structure in a 30 minute interval containing the DPPs that are shown in Figures 5 and 6. The corresponding transition region is denoted by the region bounded by two red vertical lines. The upstream and downstream are marked using the horizontal lines for which the start and end points represent the corresponding front and rear boundaries, and the location labels the average dynamic pressure in the upstream and downstream regions. It can be seen that the code does not falsely identify any events since the selection criteria should be satisfied according to the above detection algorithm. The transition region determined is able to capture all the large-scale pressure variances as expected although the changing forms of dynamic pressure are very complicated for some events (see cases (9), (10), and (14) in Figure 7, and cases (3), (4), (7), (10), (12) in Figure 8) and in the selected upstream and downstream regions, the dynamic pressure is relatively quiet as defined. This result validates the effectiveness of the code.

Figures 9 and 10 present the high-resolution dynamic pressure data during interval A and interval B in 15 subfigures (4 hr data in each subfigure in Figure 9 and 2 hr data in each subfigure in Figure 10). The red solid lines mark the medium position of the transition region of each code-given DPP. By visual inspection from Figures 9 and 10, it seems that some potential DPPs with an abrupt change in solar wind dynamic pressure are not found by the code (see the green dashed lines in each figure). Then we carefully examine the dynamic

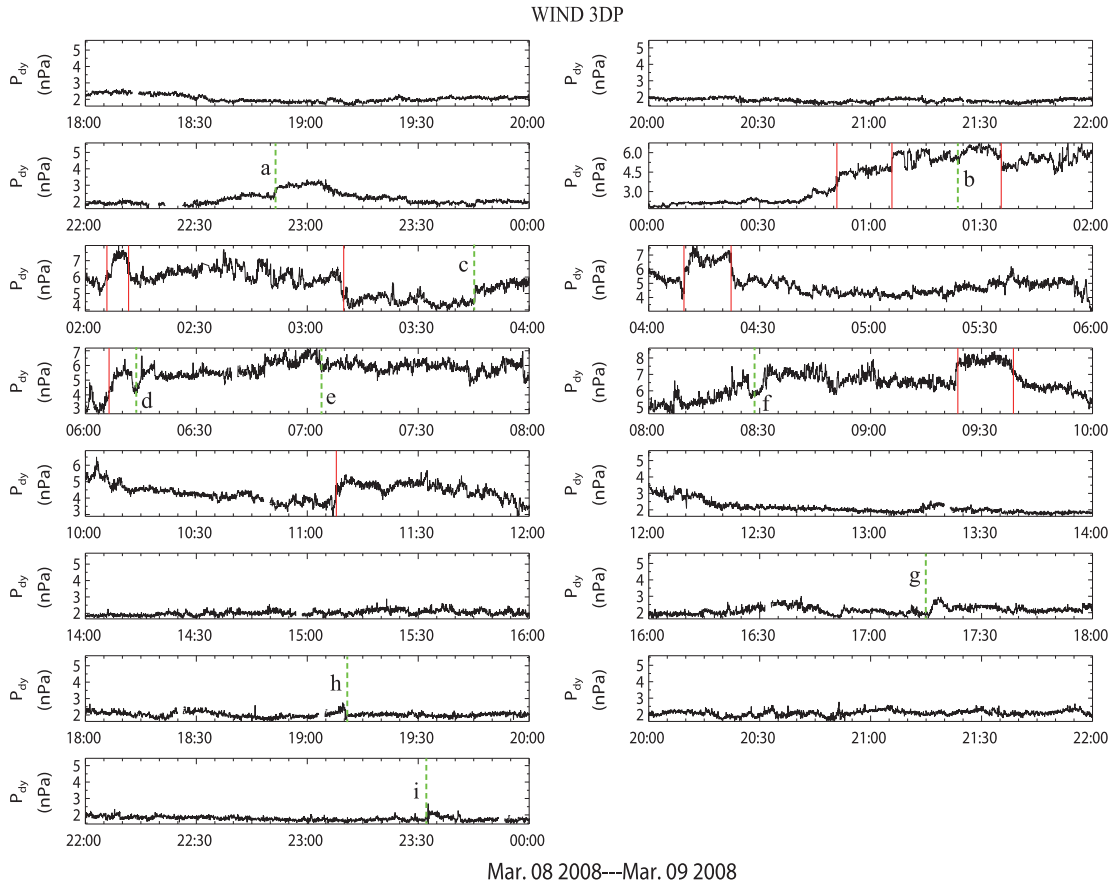

Figure 10. Dynamic pressure data from the *Wind* 3DP in the interval between 00 UT on 2008 March 8 and 24 UT on 2008 March 9 shown in 15 subfigures. The code-detected DPPs are denoted with red lines. The candidate DPPs from visual inspection are denoted with green lines.

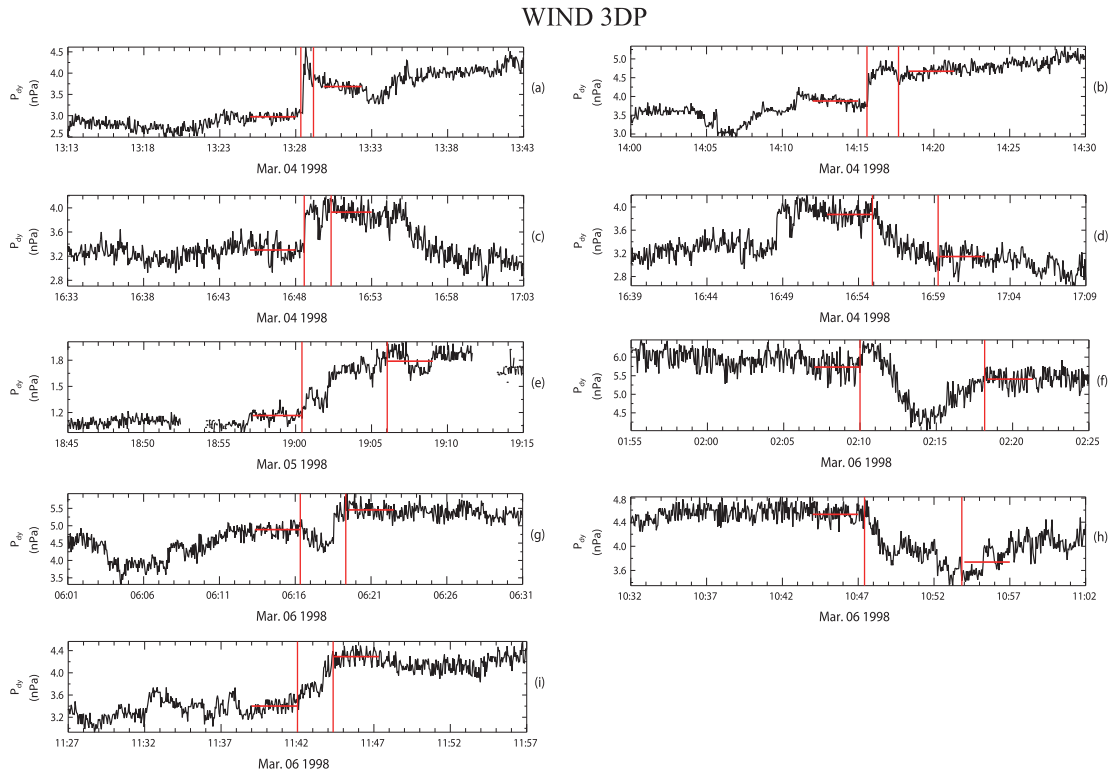

Figure 11. Fine dynamic pressure variation in a 30 minute window including each DPP candidate determined from visual inspection in Figure 8. The upstream, transition region, and downstream are given from experience.

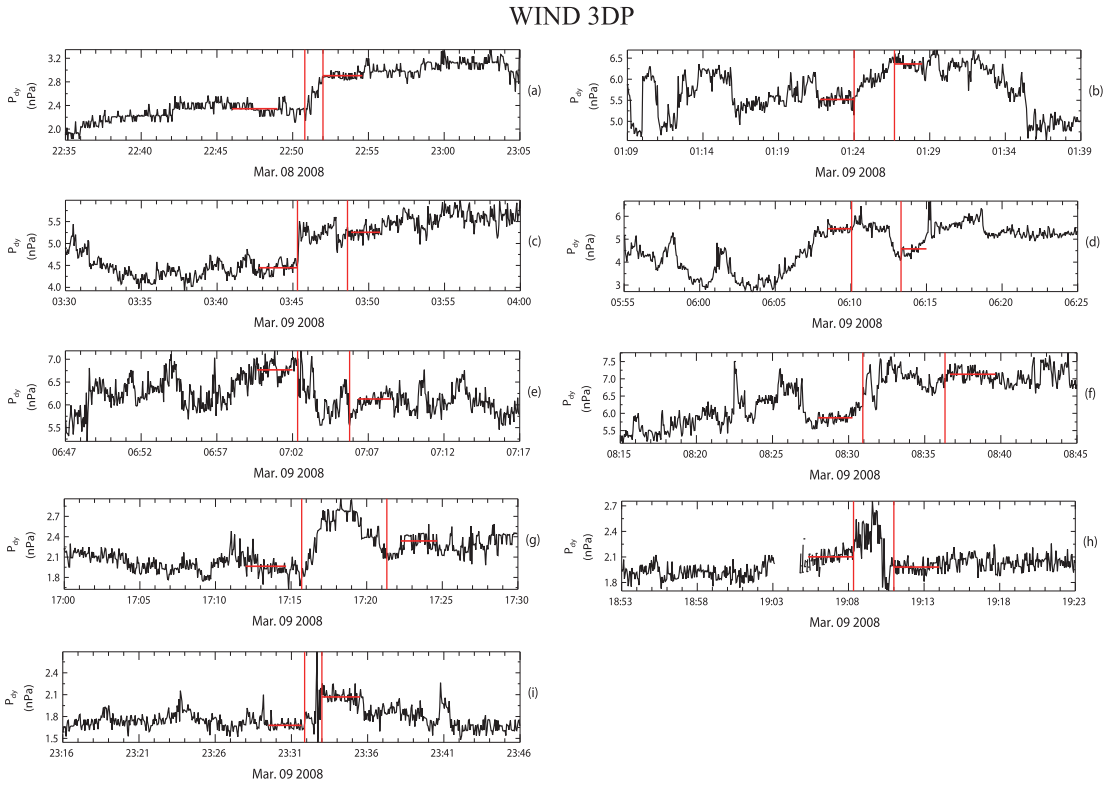

Figure 12. Fine dynamic pressure variation in a 30 minute window including each DPP candidate determined from visual inspection in Figure 9. The upstream, transition region, and downstream are given from experience.

pressure variance for each seemingly missed case and determine its transition region, upstream, and downstream region from experience. Figures 11 and 12 show the fine structure of dynamic pressure variance for each case. However, through quantitative study, it is found that the criterion given above is not met for each case. The reasons why they are missed by the code include the following. (1) Although the pressure variation amplitude may exceed 1 nPa, its change amplitude from upstream to downstream is less than 1 nPa; for example, cases (a)–(d), (g), (i) in Figure 11 and cases (a)–(e), (h), (i) in Figure 12. (2) The thickness of the transition region is larger than 5 minutes; for example, cases (e), (f), (h) in Figure 11 and cases (f), (g) in Figure 12. (3) The fluctuation of dynamic pressure in the upstream or downstream is too large relative to the pressure change from upstream to downstream; for example, cases (e), (h) in Figure 11. In this batch program, since we adopt the same selection criteria, it is inevitable to miss some events that do not meet the selected criteria but can be identified by changing the criteria parameters. The criteria parameters need to be given beforehand based on experience according to the research problem and data set.

4. SUMMARY AND DISCUSSIONS

With the motivation to rapidly and automatically identify the numerous DPPs from the solar wind data for further research, we have developed a fully automated searching procedure by providing a three-step hunting algorithm. The procedure has been applied to the high-resolution plasma data from the *Wind* spacecraft in 1996–2008 to test its effectiveness. It is found that the program works well in all types of solar wind. Due to its less expensive computational cost, the code is very efficient. For the high resolution solar wind data, the code is capable of: (1) correctly identifying the DPPs, (2) functionally determining their transition region where abrupt dynamic pressure changes occur, (3) and simultaneously selecting representative preceding and succeeding regions as the upstream and downstream.

The code can be applied to other data sets with different data rates. For solar wind measurements with low time resolution, the fine plasma structures of the transition region of DPPs is smoothed since the dynamic pressure changes usually occur on timescales of seconds to minutes. Under these circumstances, it is not necessary to determine the transition region from the data. When applying our code to low-resolution data sets, the third step of the algorithm can be ignored. The upstream and downstream of each identified DPP can be determined by the first two-step inspection.

From nearly 20 yr of observations, thousands of DPPs have been detected by the *Wind* spacecraft. Our code is useful for identifying these huge samples and determining the magnetic field and plasma parameters in a rapid way. In the near future, we will carry on a statistical study of these observation samples and hope to reveal some important scientific problems related to the DPPs, such as the origin of DPPs in the solar wind and their evolution; the relationship between the DPPs and the small- and large-scale solar wind disturbances and the global responses in the magnetosphere–ionosphere coupling system.

We would like to thank the NASA CDAWEB for providing the public *Wind* 3DP, MFI, and SWE data. This work is jointly supported by the National Basic Research Program of China (Grant No. 2012CB825601), the National Natural Science Foundation of China (41231068, 41174152, 41374188, 41304146, 41375045), and the Specialized Research Fund for State Key Laboratories.

REFERENCES

Boudouridis, A., Zesta, E., Lyons, R., Anderson, P. C., & Lummerzheim, D. 2003, JGRA, 108, 8012
Chua, D., Parks, G., Brittnacher, M., et al. 2001, JGRA, 106, 5945
Collier, M. R., Slavin, J. A., Lepping, R. P., et al. 1998, JGRA, 103, 17
Dalin, P. A., Zastenker, G. N., Paularena, K. I., & Richardson, J. D. 2002, AnGeo, 20, 293–9
Fairfield, D. H., & Jones, J. 1996, JGRA, 101, 7785
Kim, K.-H., Cattell, C. A., Lee, D.-H., et al. 2004, JGRA, 109, 4219
Lee, D. Y., & Lyons, L. R. 2004, JGRA, 109, A04201
Lee, D. Y., Lyons, L. R., & Reeves, G. D. 2005, JGRA, 110, 9213
Lee, D. Y., Lyons, L. R., & Yumoto, K. 2004, JGRA, 109, A04202
Li, X., Baker, D. N., Elkington, S., et al. 2003, JASTP, 65, 233
Lin, R. P., Anderson, K. A., Ashford, S., et al. 1995, SSRv, 71, 125
Liou, K., Newell, P. T., Meng, C.-I., Wu, C.-C., & Lepping, R. P. 2004, JGRA, 109, 6306
Lyon, J. G. 2000, Sci, 228, 1987
Lyons, L. R., Lee, D.-Y., Wang, C.-P., & Mende, S. B. 2005, JASTP, 110, 8208
Lyons, L. R., Zesta, E., Samson, J. C., & Reeves, G. D. 2000, GeoRL, 27, 3237
Neugebauer, M. 2006, JGRA, 111, A04103
Ostapenko, A. A., & Maltsev, Y. P. 1998, GeoRL, 25, 261
Riazantseva, M. O., Khabarova, O. V., Zastenker, G. N., & Richardson, J. D. 2007, AdSpR, 40, 1802
Riazantseva, M. O., Zastenker, G. N., & Richardson, J. D. 2005, AdSpR, 35, 2147
Richardson, I. G., & Cane, H. V. 2012, JSWSC, 2, A02
Russell, C. T., Ginskey, M., & Petrinec, S. M. 1994, JGR, 99, 253
Saka, O., & Kitamura, T. 1976, P&SS, 24, 1043
Sanny, J., Tapia, J. A., Sibeck, D. G., & Moldwin, M. B. 2002, JGRA, 107, 1443
Wang, C., Liu, J. B., & Huang, Z. H. 2007, JGRA, 112, A12210
Wing, S., Sibeck, D. G., Wiltberger, M., & Singer, H. 2002, JGRA, 107, 1222
Wu, B. H., Mandt, M. E., Lee, L. C., & Chao, J. K. 1993, JGRA, 98, 21297
Zastenker, G. N., & Borodkova, N. L. 1991, JGG, 43, 89
Zesta, E., Singer, H. J., Lummerzheim, D., et al. 2000, in Geophysical Monograph 118, Magnetospheric Current Systems, ed. S. Ohtani, R. Fuji, M. Hesse, & R. L. Lysak (Washington, DC: AGU), 217
Zhou, X. Y., Zhou, X. Z., Angelopoulos, V., et al. 2013, JGRA, 118, 3173
Zong, Q. G., Zhou, X. Z., Wang, Y. F., et al. 2009, JGRA, 114, A10204
Zuo, P. B., Wei, F. S., & Feng, X. S. 2006, GeoRL, 33, L15107